8-12-2004

# Comparison of Basis-Vector Selection Methods for Target and Background Subspaces as Applied to Subpixel Target Detection

Peter Bajorski
*Rochester Institute of Technology*

Emmett J. Ientilucci
*Rochester Institute of Technology*

John Schott
*Rochester Institute of Technology*



Recommended Citation
Peter Bajorski, Emmett J. Ientilucci, John R. Schott, "Comparison of basis-vector selection methods for target and background subspaces as applied to subpixel target detection", Proc. SPIE 5425, Algorithms and Technologies for Multispectral, Hyperspectral, and Ultraspectral Imagery X, (12 August 2004); doi: 10.1117/12.542460; https://doi.org/10.1117/12.542460

# Comparison of Basis-Vector Selection Methods for Target and Background Subspaces as Applied to Subpixel Target Detection

Peter Bajorski[a], Emmett J. Ientilucci[b], John R. Schott[b]

[a]Center for Quality and Applied Statistics, Rochester Institute of Technology, Rochester, NY, USA
[b]Digital Imaging and Remote Sensing Laboratory, Rochester Institute of Technology Rochester, NY USA

## ABSTRACT

This paper focuses on comparing three basis-vector selection techniques as applied to target detection in hyperspectral imagery. The basis-vector selection methods tested were the singular value decomposition (SVD), pixel purity index (PPI), and a newly developed approach called the maximum distance (MaxD) method. Target spaces were created using an illumination invariant technique, while the background space was generated from AVIRIS hyperspectral imagery. All three selection techniques were applied (in various combinations) to target as well as background spaces so as to generate dimensionally-reduced subspaces. Both target and background subspaces were described by linear subspace models (*i.e.*, structured models). Generated basis vectors were then implemented in a generalized likelihood ratio (GLR) detector. False alarm rates (FAR) were tabulated along with a new summary metric called the average false alarm rate (AFAR). Some additional summary metrics are also introduced. Impact of the number of basis vectors in the target and background subspaces on detector performance was also investigated. For the given AVIRIS data set, the MaxD method as applied to the background subspace outperformed the other two methods tested (SVD and PPI).

**Keywords:** Hyperspectral, Subpixel Target Detection, Endmember, Basis Vector, Subspace, AVIRIS

## 1. INTRODUCTION

This paper introduces a method for detection of subpixel targets in image spectrometer data cubes. It is based on the premise that we know what the target is and can characterize it in terms of its reflectance spectrum. Furthermore, we assume the target may exist at spatial scales such that it will present itself as a *fraction* of a pixel and that it may exist in a significant number of pixels (more specifically we can't assume that we can insure that a significant region of the scene does not contain any targets). We desire a data processing approach that can mitigate atmospheric and illumination effects such that atmospheric correction is not a required prerequisite for the method. The approach presented here involves defining a target spectral subspace that is common across the wide range of atmospheric illumination and viewing conditions that might exist in the scene (*i.e.,* the target subspace is invariant to environmental changes within the scene). The target may manifest itself at different locations within this subspace but is not expected to appear outside the subspace. We then introduce a method to characterize a background subspace using the same convex hull geometry used to define the target subspace (*i.e.,* the target and background subspaces are defined in a common spectral space but ideally there is little or no overlap between the two subspaces). We then introduce a subpixel target detection algorithm that is based on how well each pixel spectrum can be described by either a set of background basis vectors or a combination of target and background basis vectors. The result is a subpixel target detection algorithm that only requires the target spectrum and a radiance image cube (*i.e.,* an image spectrometer data set calibrated into sensor reaching

Further Information:
pxbeqa@ritvax.isc.rit.edu, (585)475-7889, 98 Lomb Memorial Drive, Rochester, NY 14623-5604
emmett@cis.rit.edu, (585)475-7778, 54 Lomb Memorial Drive, Rochester, NY 14623-5604
schott@cis.rit.edu, (585)475-5170, 54 Lomb Memorial Drive, Rochester, NY 14623-5604



Algorithms and Technologies for Multispectral, Hyperspectral, and Ultraspectral Imagery X, edited by Sylvia S. Shen, Paul E. Lewis, Proceedings of SPIE Vol. 5425 (SPIE, Bellingham, WA, 2004) · 0277-786X/04/$15 · doi: 10.1117/12.542460

radiance). The performance of the resulting algorithm is shown for an AVIRIS image. These results demonstrate the potential of the approach showing very good background suppression (low false alarms) and a high degree of target detection.

## 2. THEORY AND APPLICATION

### 2.1. The Invariant Approach and Physics Based Modeling

In target detection, we often seek to atmospherically correct hyperspectral imagery so as to convert sensor reaching radiance to ground leaving spectral reflectance. Once the imagery has been corrected, detection algorithms are used to compare image reflectances to library or measured reflectances in search of a desired target. Another approach that mitigates atmospheric and illumination effects involves the creation of an *invariant* target space that spans the potential variability of the target as seen by the sensor.[1] This approach involves defining a (sensor-reaching) target radiance space that is common across a wide range of atmospheric illumination and viewing conditions that might exist in the scene. It can be shown that the target may only occupy a relatively small portion of the space and can be described by a small set of basis vectors that describe a target *subspace*. It is the selection and comparison of these basis vectors (in a target detection scheme) which is the focus of this paper.

In order to create a target space we need to know how the atmospheric and illumination conditions will affect the target reflectance as it propagates through the atmosphere to the sensor. Schott[2] derives a relationship for the spectral radiance reaching an airborne or satellite sensor which can be expressed in simplified form as

$$L_p(\lambda) = \int_{\lambda} \beta_p(\lambda) \left[ \Big( GE'_s(\lambda)\tau_1(\lambda)\cos\theta + FE_d(\lambda) \Big) \tau_2(\lambda) \frac{r(\lambda)}{\pi} + L_u(\lambda) \right] \mathrm{d}\lambda \tag{1}$$

where $L_p(\lambda)$ is the effective spectral radiance in the $p^{th}$ band in units of $[Wcm^{-2}sr^{-1}\mu m^{-1}]$, $E'_s(\lambda)$ is the exoatmospheric spectral irradiance from the Sun in units of $[Wcm^{-2}\mu m^{-1}]$, $\tau_1(\lambda)$ is the transmission through the atmosphere along the Sun-target path, $\theta$ is the angle from the surface normal to the Sun, $F$ is the fraction of the spectral irradiance from the sky ($E_d(\lambda)$) incident on the target (*i.e.*, not blocked by adjacent objects), $G$ is the fraction of direct sunlight incident on the target, $\tau_2(\lambda)$ is the transmission along the target-sensor path, $r(\lambda)$ is the spectral reflectance factor for the target of interest (*i.e.*, $r(\lambda)/\pi$ is the bidirectional reflectance $[sr^{-1}]$), $L_u(\lambda)$ is the spectral path radiance $[Wcm^{-2}sr^{-1}\mu m^{-1}]$, and $\beta_p(\lambda)$ is the normalized spectral response of the $p^{th}$ spectral channel of the sensor under study where

$$\beta_p(\lambda) = \frac{\beta'_p(\lambda)}{\int \beta'_p(\lambda)\,\mathrm{d}\lambda} \tag{2}$$

with $\beta'_p(\lambda)$ being the peak normalized spectral response of the $p^{th}$ channel. Schott[2] also describes how the MODTRAN radiative transfer code[3] can be used to solve for each of the radiometric terms in Eq. (1) (*i.e.*, $E'_s(\lambda), \tau_1(\lambda), \tau_2(\lambda), E_d(\lambda), \text{and } L_u(\lambda)$) given a set of atmospheric and illumination descriptors. Once the terms are solved for, the spectral radiance target vector, $\mathbf{x}$ observed by a $p$-channel sensor can be expressed as

$$\mathbf{x} = [L_1(\lambda), L_2(\lambda), \ldots, L_p(\lambda)]^T. \tag{3}$$

Similarly, a range of possible target vectors can also be be generated by using the MODTRAN radiation propagation model. By changing the inputs to MODTRAN to span a range of variables representing atmospheric, illumination and viewing conditions, a wide range of potential target spectral vectors can be generated from a single target reflectance spectrum.

### 2.2. Structured Models

For the purpose of sub-pixel target detection, we use a geometric approach to model spectral variability that leads to *structured models*. An overview of target detection approaches and their classification has been published throughout the literature.[4,5]

### 2.2.1. Model Formulation

Let us consider an image consisting of $N$ pixels. Each pixel is represented by a $p$-dimensional vector of spectrum $\mathbf{x}_i$, where $p$ is the number of spectral channels or bands, and $i = 1, 2, \ldots, N$. We assume the following structured model:

$$\mathbf{x}_i = \mathbf{T}\mathbf{a}_i + \mathbf{B}\mathbf{b}_i + \boldsymbol{\epsilon}_i \tag{4}$$

where $\mathbf{T}$ is a matrix of target basis vectors, $\mathbf{B}$ is a matrix of background basis vectors, and $\mathbf{a}_i$ and $\mathbf{b}_i$, are unknown weighting vectors. The vector $\boldsymbol{\epsilon}_i$ represents approximation errors, which can be due to noise in the data or modeling error (or both). If an endmember selection method (such as PPI or MaxD) is used on the background, then the resulting basis vectors are endmembers representing real materials present in the image. The vector $\mathbf{b}_i$ represents the abundances of those materials in the given pixel $\mathbf{x}_i$. Conceptually, one would like to have endmembers representing pure materials though this is not a necessity for the purpose of target detection. The target endmembers, however, should not be interpreted as real materials. Consequently, we can think of the target endmembers as basis vectors that attempt to describe the whole target space through their linear combinations. Clearly, the basis vectors generated by an SVD approach cannot be regarded as endmembers. Their interpretation is similar to that of the target endmembers, that is, the target (or background) space is described by linear combinations of the SVD basis vectors.

If certain assumptions about $\boldsymbol{\epsilon}_i$ are made, some elegant results can be obtained, as described in Sec. (2.2.2). Unfortunately, such assumptions are rarely met in practice. The results presented in this paper do not require any assumptions about $\boldsymbol{\epsilon}_i$ . However, the idea is to have the modeling error be as small as possible. To this end, the unknown vectors $\mathbf{a}_i$ and $\mathbf{b}_i$, are usually estimated using a least-squares method, which is also implemented in this paper.

### 2.2.2. Target Detection in Structured Models

The structured model in Eq. (4) may arise in one of two scenarios, *i*) we are trying to detect several targets (columns of $\mathbf{T}$) at once. A pixel is identified as containing the target if at least one of the targets is present and *ii)* the exact spectrum of the target is unknown. The target space is known to be defined by linear combinations of target basis vectors generated by various illumination and atmospheric conditions. In this paper, we concentrate on the latter scenario where we have an estimate of the target subspace. We now make the following assumptions:

1. The matrix $\mathbf{T}$ is a known matrix of the target basis vectors (independent of the image spectra $\mathbf{x}_i, i = 1, 2, \ldots, N$).
2. The matrix $\mathbf{B}$ is a known matrix of the background basis vectors (independent of the image spectra $\mathbf{x}_i, i = 1, 2, \ldots, N$).
3. The vectors $\boldsymbol{\epsilon}_i$ follow the multivariate normal distribution such that $\boldsymbol{\epsilon} \sim N(\mathbf{0}, \sigma^2\mathbf{I})$.

Under these assumptions, optimal target detectors can be defined. As we will see, some of these assumptions are not usually fulfilled in real data. However, the constructed detectors can still be used even though they are not guaranteed to have optimal properties.

Assumption (1) is realistic because $\mathbf{T}$ represents the target space which is constructed based on a known target spectrum and the illumination invariant technique described previously. That is, it is independent of the image spectra. Assumption (2) is not realistic because $\mathbf{B}$ is derived directly from the image spectra. Lastly, the assumption about normality of the residuals is typically not met in real data. This result is widely recognized in current literature.[6]

For notation purposes, we will concentrate on a fixed pixel spectrum and omit the index $i$. Consequently Eq. (4) becomes

$$\mathbf{x} = \mathbf{T}\mathbf{a} + \mathbf{B}\mathbf{b} + \boldsymbol{\epsilon}. \tag{5}$$

The target detection problem can be defined as a hypothesis-testing problem for testing the null hypothesis that all values in vector $\mathbf{a}$ are zero. That is,

$$H_0 : \mathbf{a} = \mathbf{0} \tag{6}$$

where $\mathbf{0}$ is a vector of zeros, versus the alternative hypothesis

$$H_1 : \mathbf{a} \neq \mathbf{0}. \tag{7}$$

Due to physical constrains, the coordinates of the vector $\mathbf{a}$ could be required to be positive (or even sum to 1), however, such constraints are not explicitly needed in the detection methods presented in this paper. Under assumptions (1-3), the generalized likelihood ratio (GLR) test for testing $H_0$ versus $H_1$ is based on the following statistic

$$GLR(\mathbf{x}) = \left( \frac{\mathbf{x^T P_B^\perp x}}{\mathbf{x^T P_Z^\perp x}} \right)^{p/2} \tag{8}$$

where $\mathbf{Z} = [\mathbf{T}, \mathbf{B}]$ is a matrix consisting of all columns of $\mathbf{T}$ and $\mathbf{B}$, and $\mathbf{P_Y^\perp}$ (for $\mathbf{Y}$ equal to $\mathbf{B}$ or $\mathbf{Z}$) is the matrix of the projection onto the space orthogonal to the space generated by columns of $\mathbf{Y}$. That is,

$$\mathbf{P_Y^\perp} = \mathbf{I} - \mathbf{Y}(\mathbf{Y^T Y})^{-1}\mathbf{Y^T} \tag{9}$$

where $\mathbf{I}$ is the identity matrix. The GLR statistic is a monotonic function of a matched subspace detector (MSD)[7]

$$MSD(\mathbf{x}) = \frac{\mathbf{x^T}(\mathbf{P_B^\perp} - \mathbf{P_Z^\perp})\mathbf{x}}{\mathbf{x^T P_Z^\perp x}}. \tag{10}$$

More specifically,

$$GLR(\mathbf{x}) = (MSD(\mathbf{x}) + 1)^{p/2}. \tag{11}$$

That is, the MSD is equivalent to the GLR. Consequently, the target detector to be used in this paper will be the MSD. The MSD is also called a partial F-statistic in statistics.

It is a well-known result in statistics that, under assumptions (1-3), the MSD follows an F-distribution under the null hypothesis $H_0 : \mathbf{a} = \mathbf{0}$, and a non-central F-distribution under the alternative hypothesis $H_0 : \mathbf{a} \neq \mathbf{0}$. These results, in the context of remote sensing and signal detection, are presented throughout the literature.[6,7] Consequently, if assumptions (1-3) held in practice, one could find a threshold value $f$ for detecting the target when $MSD(\mathbf{x}) > f$ , and theoretical receiver operator characteristic (ROC) curves could easily be constructed. Unfortunately, assumptions (2-3) do not usually hold in practice, which causes difficulties with choosing the appropriate threshold value $f$. To resolve this issue, we assess the performance of the basis vector selection methods using the observed ROC curves (*cf.* Sec. 3.2).

## 2.3. Approaches to Generating Basis Vectors

In this section, we briefly describe three basis vector selection methods used in this paper.

### 2.3.1. Singular Value Decomposition (SVD)

Let us now define a $p \times N$ matrix $\mathbf{Y}$ of all image pixels (given as columns) and consider the singular value decomposition (SVD) of $\mathbf{Y}$:

$$\mathbf{Y} = \mathbf{U}\mathbf{D}\mathbf{V}^T \tag{12}$$

where $\mathbf{U}_{p\times p} = [u_j]_{j=1,\ldots,p}$ is the matrix of eigenvectors of $\mathbf{Y}\mathbf{Y}^T$ and $\mathbf{D}$ is the diagonal matrix of singular values $\sigma_i$, such that $\sigma_1 \geq \sigma_2 \geq \ldots \geq \sigma_p \geq 0$. Healey and Slater[1] use the first $r$ columns of $\mathbf{U}$, that is, $\mathbf{B} = [u_1, \ldots, u_r]$, as the background basis vectors. If some of the image pixels are easily identified as containing target (for instance, by using the spectral angle mapper[8] algorithm), they are removed from the matrix $\mathbf{Y}$ before the SVD is calculated. Some criteria for choosing the number of basis vectors $r$ are presented in Thai *et al.*[9] They are mostly based on the percent of variability explained by the first $r$ vectors. Since the SVD is very efficient in capturing the directions (vectors) explaining most of the variability, a relatively small number of basis vectors tends to explain more than 99.99% of the overall variability. Unfortunately, it is difficult to decide how much explained variability is sufficient for the purpose of target detection.

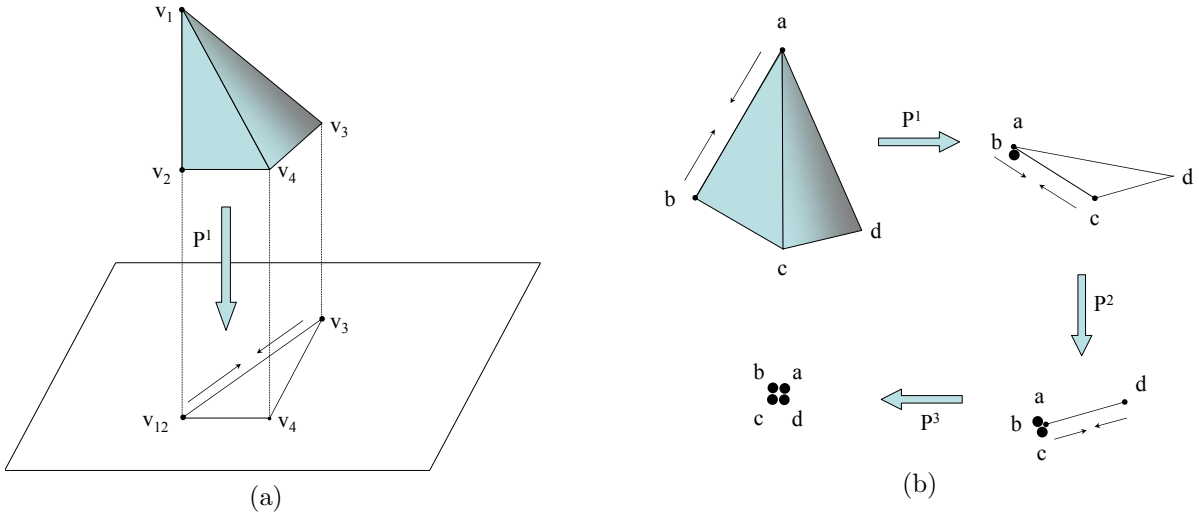


**Figure 1.** Illustration of (a) the preservation of vertices of a simplex through projection of a data set onto the difference in two vertices of a simplex and (b) the concept of maximum distance determination and sequential projection to find the vertices of a simplex spanning the data space.

### 2.3.2. Pixel Purity Index (PPI)

In the PPI method,[10] pixel vectors are repeatedly projected into random directions. The coordinates of the direction vectors are generated using a standard normal distribution, so that all directions in the $p$-dimensional space are equally likely. Once all projections on a given random vector are calculated, two extreme projections are identified (the shortest and the longest one). Each of the two pixels associated with the two extreme projections receives one extremity score. This process is repeated many times (150,000 iterations in this paper), and a desired number of pixels with the top extremity scores are identified as the set of endmembers.

One problem with the PPI method is that clusters of pixels that are close to each other tend to receive large extremity scores. Consequently, identification of those similar pixels is needed, so that only one pixel per cluster is represented in the final set of endmembers. Such clustering was also implemented in this paper.

### 2.3.3. Maximum Distance Method (MaxD)

The maximum distance (MaxD) method is a new endmember selection method suggested by Lee[11] and further investigated by Schott.[12] The method consists of finding *native* (*i.e.,* vectors that are in the original image space) endmember vectors that best approximate a simplex defining the target subspace. The technique starts with identifying two pixels, one with the largest magnitude vector (denoted by $\mathbf{v}_1$) and one with the smallest magnitude (denoted by $\mathbf{v}_2$). Next, all pixel vectors are projected along $\mathbf{v}_1 - \mathbf{v}_2$ onto the subspace orthogonal to $\mathbf{v}_1 - \mathbf{v}_2$ [*cf.* Figure 1(a)]. In this projection, both $\mathbf{v}_1$ and $\mathbf{v}_2$ project on the same point (which we will call $\mathbf{v}_{12}$). Then, the distance between $\mathbf{v}_{12}$ and the remaining projections are calculated. The pixel with the maximum distance to $\mathbf{v}_{12}$ is the third endmember (denoted by $\mathbf{v}_3$). All projected points are now projected along $\mathbf{v}_{12} - \mathbf{v}_3$. The resulting end-member is denoted by $\mathbf{v}_{123}$. The process is repeated until a desired number of endmembers is identified. If this process is continued until $(p+1)$ endmembers are identified, all projected points reduce to one point, and the process can no longer be continued. That is, we can identify up to $(p+1)$ endmembers using MaxD, which is not a limitation in practice when working with hyperspectral images. Additionally, the MaxD method is very fast computationally and is fully automated.

## 2.4. Metrics for Evaluating Target Detection Methods

As explained in Sec. 2.2.2, the performance of the basis vector selection techniques is evaluated based on observed ROC curves. The curve is a plot of detection rate (DR) versus false alarm rate (FAR). We specifically use the term "detection rate" rather than "probability of detection" because these results are based on the observed frequency of detecting the target rather than on theoretical calculations of probabilities.

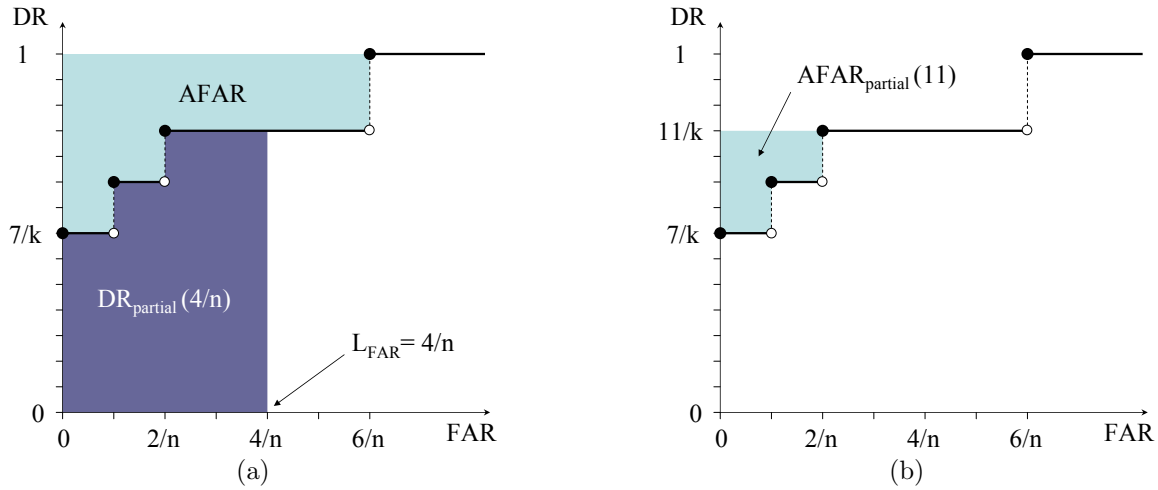


**Figure 2.** Example ROC curves illustrating summary metrics for (a) AFAR and ADR (up to a FAR value of $4/n$) and (b) partial AFAR (for $m$ out of all $k$ targets).

Due to a large number of cases considered (*cf.* Sec 3.2), it would not be effective to simply plot the observed ROC curves (*e.g.,* for our analysis we would need 1440 curves). Hence, there was a need to use some summary metrics. In addition to summarizing detection rates (DR) at several FAR levels, we also used a new summary metric called the average FAR (AFAR). In order to define AFAR, let us assume that there are $k$ pixels in the image that contain the target. The observed ROC curve is fully described by $k$ numbers $r_i, i = 1, \ldots, k$, where $r_i$ is the lowest FAR to achieve $i/k$ detection rate (DR). The AFAR is defined as

$$AFAR = \frac{1}{k} \sum_{i=1}^{k} r_i. \tag{13}$$

If the observed ROC curve is plotted as a step function then

$$ROC(x) = \min\{i/n : r_i \leq x\}, \text{ for } 0 \leq x \leq 1 \tag{14}$$

where $n$ is the total number of pixels in the image. The AFAR is now the area above the observed ROC curve (to be more precise, the area between the observed ROC curve and a DR level of 1). Consequently, AFAR can also be expressed as one minus the area under the observed ROC curve. As an example, consider a detector, $D(x)$ and its sorted (descending) values for all $n = 10000$ pixels. Assume that the the top 20 values are labelled as follows:

$$\underbrace{T, T, \ldots, T}_{7\, occurances},\ \boldsymbol{F},\ T,\ T,\ \boldsymbol{F},\ T,\ T,\ \boldsymbol{F,F,F,F},\ T,\ T,\ T,\ \ldots$$

where the label $T$ is for a target pixel and $F$ a non-target pixel or false alarm. Subsequently, all the remaining detector values are non-target pixels. This produces the ROC curve shown in Figure 2. For this example, following Eq. (13), we have $k = 14$ and $r_1 = r_2 = \ldots = r_7 = 0$. Additionally, $r_8 = r_9 = 1/n$, $r_{10} = r_{11} = 2/n$ and $r_{12} = r_{13} = r_{14} = 6/n$. The AFAR is then,

$$AFAR = \frac{1}{14}\left(\frac{1}{n} + \frac{1}{n} + \frac{2}{n} + \frac{2}{n} + \frac{6}{n} + \frac{6}{n} + \frac{6}{n}\right) = \frac{12}{7n}.$$

The result of this calculation can be seen in Figure 2(a) as the shaded region above the ROC curve.

The AFAR is a convenient overall measure of detection performance. Sometimes, we might be interested in detection of only a certain fraction of targets (for example, $m$ out of all $k$ targets). In such cases, we can define the partial AFAR as

$$AFAR_{partial}(m) = \frac{1}{k} \sum_{i=1}^{m} r_i. \tag{15}$$

Equation (15) contains the factor $1/k$ rather than $1/m$ to keep the interpretation consistent with that of the AFAR. In keeping with our example, we let $m = 11$ and calculate the partial AFAR as,

$$AFAR_{partial}(11) = \frac{1}{14}\left(\frac{1}{n} + \frac{1}{n} + \frac{2}{n} + \frac{2}{n}\right) = \frac{3}{7n}.$$

This area calculation is illustrated in Figure 2(b) as the shaded region between $7/k$ and $11/k$.

If we are interested in the detector performance only up to a certain level of FAR, we can define the partial DR as

$$DR_{partial}(L_{FAR}) = \int_0^{L_{FAR}} ROC(x)\, \mathrm{d}x \tag{16}$$

where $L_{FAR}$ is the desired FAR level. Since we are considering the observed ROC curve as a step function, alternative formulas for $DR_{partial}$ are

$$DR_{partial}(L_{FAR}) = \frac{1}{k}\sum_{i=1}^{m}(L_{FAR} - r_i) \tag{17}$$

and

$$DR_{partial}(L_{FAR}) = \frac{m}{k}L_{FAR} - AFAR_{partial}(m) \tag{18}$$

where $m = k \cdot ROC(L_{FAR})$. Setting $L_{FAR} = 4/n$, using Eq. (18), and referring back to our example above, we have

$$DR_{partial}(4/n) = \frac{11}{14} \cdot \frac{4}{n} - \frac{3}{7n} = \frac{19}{7n}.$$

This last metric is illustrated in Figure 2(a) as the shaded region below the ROC curve.

## 3. RESULTS

### 3.1. Experimental Design

The basis-vector selection algorithms were implemented on a cluttered AVIRIS urban scene in Rochester, NY near the Lake Ontario shoreline (*cf.* Figure 3). A $100 \times 100$ pixel region was selected for evaluation [*cf.* Figure 3(b)]. This section had a wide range of natural and man-made clutter including a mixture of commercial/warehouse and residential neighborhoods to add a wide range of spectral diversity. The target of interest was a reddish brown paint used on basketball and tennis court playing surfaces, as can be seen in Figures 3(c-d). From the $100 \times 100$ image, 14 pixels were identified as target, 7 on the basketball court and 7 on the tennis court. Prior to processing, invalid bands, due to atmospheric water absorption, were removed reducing the overall dimensionality to 152 bands.

Basis-vector selection methods were also implemented on a MODTRAN generated target space. The target space was created by first obtaining a ground measurement of the reddish brown surface with a field spectrometer. This signature was then implemented in the physics based model introduced in Eq. (1). MODTRAN was used to solve for the various atmospheric parameters, in which variables such as aerosol, pressure depth, and water vapor were varied. This created an overall target space of 720 vectors $\times$ 152 bands.

### 3.2. Results Using AVIRIS Data

In this section, we present numerical results on comparisons of the three basis-vector selection techniques (SVD, MaxD, and PPI). Specifically, we used each of the three techniques for generating both the target and background basis vectors. This created a total of 9 combinations. For each of the 9 combinations, we identified up to 8 target basis vectors and up to 20 background basis vectors. This created a matrix of $8 \cdot 20 = 160$ combinations (by taking the first $i = 1, \ldots, 8$ target basis vectors and $j = 1, \ldots, 20$ background basis vectors). If we wanted the observed ROC curves for all these cases, we would need $9 \cdot 160 = 1,440$ curves. Thus the motivation to develop the metrics outlined in Section 2.4.

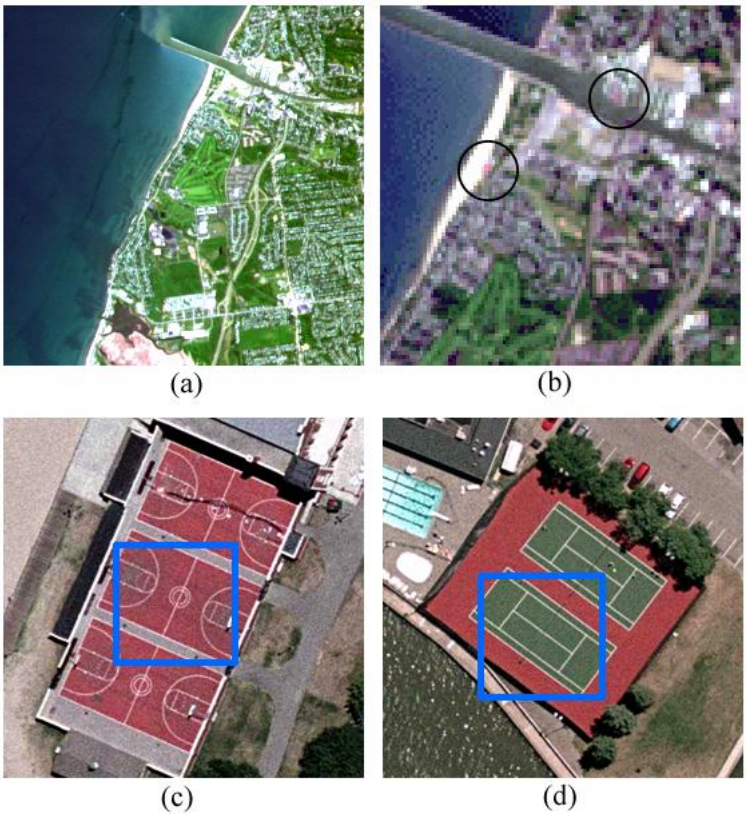


**Figure 3.** (a) AVIRIS image of Rochester, NY and Lake Ontario. (b) Actual $100 \times 100$ pixel image used for evaluation. Image contains targets of interest as illustrated by the two encircled regions. (c-d) High resolution aerial images of target regions showing a (c) red colored basketball court and a (d) red and green colored tennis court. Each high resolution image has a $20m \times 20m$ square illustrating the nominal size of an AVIRIS pixel.

As explained in Section 3.1, we identified 14 pixels as containing target spectrum. This means that $k = 14$ in the notation of Section 2.4. For each of the 1,440 cases, we calculated the 14 FAR values $r_i, i = 1, \ldots, 14$. The summary detection rate (DR) results presented in this section were inspected at several FAR levels, and the conclusions were quite similar in all cases, so we are only presenting the results at the FAR level of $10^{-4}$. In a similar fashion, results on partial AFAR and average DR were inspected, but only the results on AFAR are reported here.

Table 1 shows the optimum (largest) DR values out of the 160 cases for the combination of up to 8 target basis vectors and up to 20 background basis vectors. The results clearly show MaxD as the best method for the background basis vectors, while the dependence on the method used for the target basis vectors is quite weak. Our interpretation is that the target space is relatively simple and any of the three methods performs well. On the other hand, the background space is much more complex, and the benefits of using a more efficient method are more apparent. In a similar fashion, Table 2 shows the optimum (smallest) AFAR values out of the 160 cases. Again, MaxD performs best as the background basis-vectors selection technique.

Of course, the above best-case-scenario results are very crude measures of performance. The difficulty is that the 9 best results were obtained under different numbers of target ($i$) and background basis vectors ($j$). To gain more insight, one needs to investigate plots of DR values as a function of the number of basis vectors.

Figure 4 shows DR values as functions of the number of background basis vectors at the FAR level of $10^{-4}$, when the SVD method was used for the target space and MaxD was used for the background space. The seven curves are representative of the different number of target basis vectors. The best performance is observed in the range between 13 and 19 background basis vectors using at least 3 target basis vectors. Similar detection rate

**Table 1.** Best (largest) detection rates (DR) for up to 8 target and 20 background basis vectors at FAR of $10^{-4}$. Next to each DR entry, in parenthesis $(i, j)$, are the number of target $(i)$ and background $(j)$ basis vectors used to achieve the presented DR value.

| **Target Space Method** | **Background Space Method** | | |
|---|---|---|---|
| | SVD | MaxD | PPI |
| SVD | 0.43 *(2,6)* | 0.79 *(4,17)* | 0.43 *(2,2)* |
| MaxD | 0.50 *(2,6)* | 0.71 *(3,14)* | 0.43 *(2,3)* |
| PPI | 0.50 *(2,6)* | 0.79 *(3,14)* | 0.43 *(2,3)* |

**Table 2.** Best (smallest) AFAR values $(\cdot 10^4)$ for detection of all 14 target pixels for up to 8 target and 20 background basis vectors. Next to each AFAR entry, in parenthesis $(i, j)$, are the number of target $(i)$ and background $(j)$ basis vectors used to achieve the presented AFAR value.

| **Target Space Method** | **Background Space Method** | | |
|---|---|---|---|
| | SVD | MaxD | PPI |
| SVD | 76.6 *(8,10)* | 6.5 *(2,17)* | 102.3 *(2,17)* |
| MaxD | 87.7 *(2,10)* | 8.4 *(2,15)* | 128.8 *(3,11)* |
| PPI | 54.4 *(6,9)* | 5.9 *(3,14)* | 138.9 *(2,17)* |

plots (not shown in this paper) using MaxD and PPI for target basis vector generation, and at other FAR levels, showed similar results to those found in Figure 4. Furthermore, investigation into using SVD as the method for background basis vector selection, revealed the best performance to be in the range between 6 and 13 background basis vectors. Lastly, when PPI was used as the method for the background basis vector selection, the largest detection rates were observed when using between 10 and 20 background basis vectors.

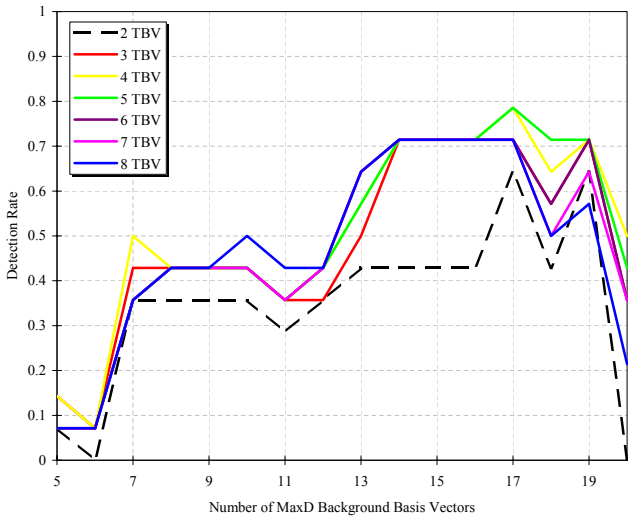


**Figure 4.** Detection rate as a function of background basis vectors at the FAR level of $10^{-4}$. The SVD method was used to generate target basis vectors.

It is apparent, from Figure 4, that the DR values are not strongly influenced by the number of target basis vectors. Consequently, we calculate the *average* detection rate (ADR) values over the range of 2 to 8 target basis vectors for SVD, MaxD, and PPI. Again, MaxD was used to generate the background basis vectors. The results of this detection rate averaging can be seen in Figure 5. It is clear that all three methods used to generate target

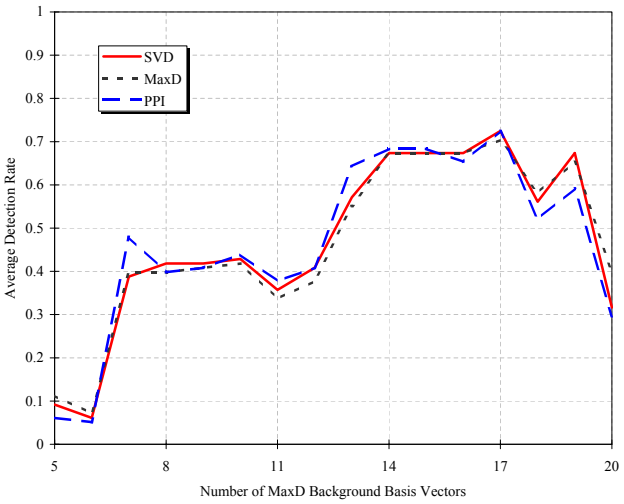


**Figure 5.** Average DR as a function of background basis vectors (FAR level of $10^{-4}$). Target basis vectors were found using SVD, MaxD and PPI.

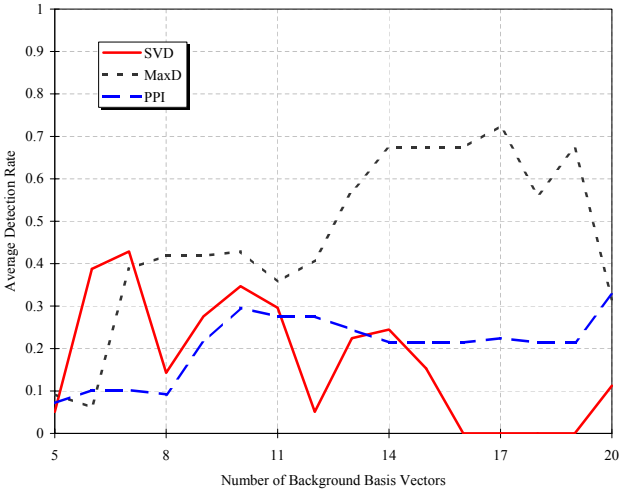


**Figure 6.** Average detection rate (ADR) as functions of the number of background basis vectors at the FAR level of $10^{-4}$. The target space method used was fixed at SVD while the background basis vectors selection methods were SVD, MaxD, and PPI.

basis vectors have similar average detection rate values and the choice of target basis vector technique has little impact on the overall results. Plots similar to Figure 5 (but not shown in this paper), which investigate SVD and PPI as the methods for the background basis vector selection, also show little impact of the target basis vector technique on the detector performance. By reporting average DR values, we are not entirely dependent on a particular number of target basis vectors.

It is apparent that all three methods, when applied to the target space, performed equally well. However, this was not the case when the methods were applied to the background. In order to make direct comparisons among the three background basis vector techniques, we fixed the target basis vector technique as SVD. We do not need to report the number of target basis vectors because of the lack of dependance stated earlier. The background basis vectors were generated with SVD, MaxD, and PPI. The results are summarized in Figure 6. We can see that in the range of 5 to 12 background basis vectors, all three methods performed about the same with the MaxD technique slightly out-performing SVD and PPI. However, the ADR values are significantly higher for MaxD over both SVD and PPI in the range of 13 to 19 background basis vectors.

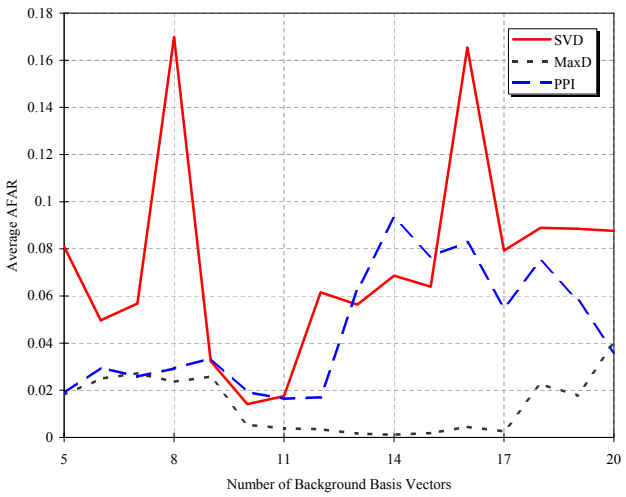


**Figure 7.** Average AFAR values as a function of the number of background basis vectors. The target space method used was fixed at SVD while the background basis vectors selection methods were SVD, MaxD, and PPI. Recall that low AFAR values indicate better performance.

The results presented thus far are in the form of DR's and averaged DR's. Analysis can also be made in terms of false alarm rates (FAR) and average FAR's (AFAR), after detecting all 14 target pixels. Further analysis on plots similar to those of Figures 4 and 6 but not presented in this paper, show that AFAR values over the range between 2 and 8 target basis vectors illustrated little impact by the number of the target basis vectors. This result was also found in evaluating DR's (*cf.* Figure 4). There is one exception, however, when PPI was used for the background space, choosing only 2 target basis vectors gave performance that was much better than that for more than 2 target basis vectors, no matter which technique was used for the target space. Since there is no significant dependency on the number of target basis vectors, we can summarize by computing an average AFAR. Figure 7 shows such a plot for comparison of the three background basis vector techniques, when the target basis vector technique was fixed as SVD. Again, we see uniformly lower false alarms over SVD and PPI when using the MaxD technique to select background basis vectors.

## 4. CONCLUSIONS AND FUTURE WORK

This paper focused on comparing the results of using 3 basis vectors selection methods as applied to hyperspectral imagery while introducing a new basis vector selection method called the maximum distance method (MaxD). Summary metrics, such as a newly developed average false alarm rate, were used to draw conclusions. All three basis vector selection techniques used for the target space were about equally good. However, MaxD outperformed both SVD and PPI when applied to the background space. Since there was no major dependency on which method to use on the target space, MaxD could be used for both background and target spaces to ensure uniformity. In general, a relatively large number of background basis vectors is recommended (larger than usually considered in the current literature). For the presented AVIRIS data set, 13 to 17 background basis vectors produce the highest detection rates, using the MaxD technique. The poor performance of SVD is surprising because SVD is by definition the most efficient way to generate subspaces explaining most of the variability in the data. We suspect that the reason for the SVD poor performance is that the SVD generated background subspace is, in fact, too large and it gets very close to the target space. More research is needed in order to develop guidelines on the optimal number of background and target basis vectors. This could be in the form of additional testing and evaluation of other hyperspectral data sets that have targets and backgrounds that are different from the AVIRIS data set tested in this paper. Additionally, this paper did not address the issue of sensor noise or data reduction via principal components (or similar), which could be the subject of future work.

## ACKNOWLEDGMENTS

This work was funded under the Office of Naval Research Multi-disciplinary University Research Initiative "Model-based Hyperspectral Exploitation Algorithm Development" #N00014-01-1-0867

## REFERENCES

1. G. Healey and D. Slater. Models and methods for automated material identification in hyperspectral imagery acquired under unknown illumination and atmospheric conditions. *IEEE Transactions on Geoscience and Remote Sensing*, 37(6):2706–2717, November 1999.
2. J.R. Schott. *Remote Sensing: The Imaging Chaing Approach.* Oxford University Press, New York, 1997.
3. A. Berk, L.S. Bernstein, and D.C. Robertson. MODTRAN: A moderate resolution model for LOWTRAN 7. Technical Report GL-TR-89-0122, Air Force Geophysics Laboratory, Hanscom AFB, MA, 1988.
4. D. Manolakis. Overview of algorithms for hyperspectral target detection: theory and practice. In *Proc. SPIE, Algorithms and Technologies for Multispectral,Hyperspectral, and Ultraspectral Imagery VIII*, volume 4725, pages 202–215, Orlando, FL, April 2002.
5. D. Manolakis and G. Shaw. Detection algorithms for hyperspectral imaging applications. *IEEE Signal Processing Magazine*, 19(1):29–43, January 2002.
6. D. Manolakis, C. Siracusa, and G. Shaw. Hyperspectral subpixel target detection using the linear mixing model. *IEEE Transactions on Geoscience and Remote Sensing*, 39(7):1392–1409, July 2001.
7. L. Scharf and B. Friedlander. Matched subspace detectors. *IEEE Transactions on Signal Processing*, 42(8):2146–2157, August 1994.
8. F.A. Kruse, A.B. Lefkoff, J.W. Boardman, K.B. Heidebrecht, A.T. Shapiro, P.J. Barloon, and A.F.H. Goetz. The spectral image processing system (SIPS) - interactive visualization and analysis of imaging spectrometer data. *Remote Sensing of Environment*, 44:145–163, 1993.
9. B. Thai, G. Healey, and D. Slater. Invariant subpixel material identification in AVIRIS imagery. In *Proc. JPL AVIRIS Workshop*, JPL Publication 99-17, Pasadena, CA, February 1999.
10. J. W. Boardman, F. A. Kruse, and R. O. Green. Mapping target signatures via partial unmixing of AVIRIS data. In *Fifth JPL Airborne Earth Science Workshop*, volume 1 of *JPL Publication 95-1*, pages 23–26, 1995.
11. K. Lee. *A subpixel scale target detection algorithm for hyperspectral imagery.* PhD dissertation, Rochester Institute of Technology, 54 Lomb Memorial Drive, Rochester, NY, 2003.
12. J.R. Schott, K. Lee, R. Raqueno, G. Hoffmann, and G. Healey. A subpixel target detection technique based on the invariance approach. To be published, 2004.